Eur. Phys. J. C (2018) 78:313
https://doi.org/10.1140/epjc/s10052-018-5796-y

THE EUROPEAN PHYSICAL JOURNAL C

Regular Article - Theoretical Physics

Cosmological model-independent test of ΛCDM with two-point diagnostic by the observational Hubble parameter data

Shu-Lei Cao[1,2], **Xiao-Wei Duan**[3], **Xiao-Lei Meng**[2], **Tong-Jie Zhang**[1,2,a]

[1] Dezhou University, Dezhou 253023, China
[2] Department of Astronomy, Beijing Normal University, Beijing 100875, China
[3] Department of Astronomy, School of Physics, Peking University, Beijing 100871, China

Received: 8 February 2018 / Accepted: 9 April 2018 / Published online: 19 April 2018
© The Author(s) 2018

Abstract Aiming at exploring the nature of dark energy (DE), we use forty-three observational Hubble parameter data (OHD) in the redshift range $0 < z \leqslant 2.36$ to make a cosmological model-independent test of the ΛCDM model with two-point $Omh^2(z_2; z_1)$ diagnostic. In ΛCDM model, with equation of state (EoS) $w = -1$, two-point diagnostic relation $Omh^2 \equiv \Omega_{\rm m}h^2$ is tenable, where $\Omega_{\rm m}$ is the present matter density parameter, and h is the Hubble parameter divided by 100 km s^{-1} Mpc^{-1}. We utilize two methods: the weighted mean and median statistics to bin the OHD to increase the signal-to-noise ratio of the measurements. The binning methods turn out to be promising and considered to be robust. By applying the two-point diagnostic to the binned data, we find that although the best-fit values of Omh^2 fluctuate as the continuous redshift intervals change, on average, they are continuous with being constant within 1 σ confidence interval. Therefore, we conclude that the ΛCDM model cannot be ruled out.

1 Introduction

Over the past few decades, there have been a number of approaches proposed to quantitatively investigate the expansion history and structure growth of the universe (see [1,2] for recent reviews). The observations of Type Ia supernovae (SNIa) [3,4] have provided ample evidence for an accelerating expansion to an increasing precision [5]. Other complementary probes support that phenomenon, including the baryon acoustic oscillation (BAO) measurements, the weak gravitational lensing, the abundance of galaxy clusters [8], the cosmic microwave background (CMB) anisotropies, the linear growth of large-scale structure [10], and the Hubble constant H_0 [11]. There are plenty of cosmological models raised to account for the acceleration phenomenon, yet the best-fit one is still uncertain.

The existence of dark energy (DE) with negative equation of state (EoS) parameter $w \equiv p_{\rm DE}/\rho_{\rm DE}$ is considered as a prevailing interpretation currently. In this context, the most popular DE model being used remains to be the simple cosmological constant cold dark matter (ΛCDM) model, with $w = -1$ at all times [12]. However, the popularity of ΛCDM model does not cover the issue that it suffers from fine-tuning and coincidence problems [13,14]. In addition, it is worth noticing about the possibility of DE with evolving EoS [15], i.e. the dynamical DE models ($w = w(z)$), such as Quintessence [$w > -1$, 16, 17], Phantom [$w < -1$, 18], K-essence [$w > -1$ or $w < -1$, 19, 20], and especially Quintom [w crossing -1, 21, 22] models. Nevertheless, it deserves more profound, physical explanations for all these models. Moreover, Zhao et al. [15] find that an evolving DE can relieve the tensions presented among existing datasets within the ΛCDM framework. Meanwhile, it is useful to introduce diagnostics based upon direct observations and capable of revealing dynamical features of DE. One of these diagnostics is $Om(z)$, which is defined as a function of redshift z [23,24], i.e.,

$$Om(z) = \frac{\tilde{h}^2(z) - 1}{(1+z)^3 - 1}, \tag{1}$$

with $\tilde{h} = \frac{H(z)}{H_0}$ and $H(z)$ denoting the Hubble expansion rate. $Om(z)$ has the property of being $\Omega_{\rm m}$ for $w = -1$ case. Moreover, Shafieloo et al. [25] modified this diagnostic to accommodate two-point situations as follows,

$$Om(z_2; z_1) = \frac{\tilde{h}^2(z_2) - \tilde{h}^2(z_1)}{(1+z_2)^3 - (1+z_1)^3}. \tag{2}$$

In this case, if $Om(z_2; z_1) \equiv \Omega_{\rm m}$ held for any redshift intervals, it would substantiate the validity of ΛCDM. In other words, the measurements of $Om(z_2; z_1) \neq \Omega_{\rm m}$ would imply

[a] e-mail: tjzhang@bnu.edu.cn

a deviation from ΛCDM and the fact that other DE models with an evolving EoS should be taken into account.

In this paper, we first introduce the measurements of the observational $H(z)$ data (OHD) and then exhibit the currently available data sets in Sect. 2. In Sect. 3, we apply two binning methods: the weighted mean and median statistics techniques to OHD, and obtain the binned OHD categorically. In Sect. 4, based on the binned OHD, we test the ΛCDM model with two-point $Omh^2(z_2; z_1)$ diagnostic. Finally, we summarize our conclusions in Sect. 5.

2 The observational $H(z)$ data sets

The OHD can be used to constrain cosmological parameters because they are obtained from model-independent direct observations. Until now, three methods have been developed to measure OHD: cosmic chronometers, radial BAO size methods [26], and gravitational waves [27]. Jimenez et al. [28] first proposed that relative galaxy ages can be used to obtain $H(z)$ values and they reported one $H(z)$ measurement at $z \sim 0.1$ in their later work [29]. Simon et al. [30] added additional eight $H(z)$ points in the redshift range between 0.17 and 1.75 from differential ages of passively evolving galaxies, and further constrained the redshift dependence of the DE potential by reconstructing it as a function of redshift. Later, Stern et al. [31] provided two new determinations from red-envelope galaxies and then constrained cosmological parameters including curvature through the joint analysis of CMB data. Furthermore, Moresco et al. [32] obtained eight new measurements of $H(z)$ from the differential spectroscopic evolution of early-type, massive, red elliptical galaxies which can be used as standard cosmic chronometers. By applying the galaxy differential age method to SDSS DR7, Zhang et al. [33] expanded the $H(z)$ data sample by four new points. Taking advantage of near-infrared spectroscopy of high redshift galaxies, Moresco et al. [34] obtained two measurements of $H(z)$. Later, they gained five more latest $H(z)$ values [35]. Recently, Ratsimbazafy et al. [36] provides one more measurement of $H(z)$ based on analysis of high quality spectra of Luminous Red Galaxies (LRGs) obtained with the Southern African Large Telescope (SALT).

On the other side, $H(z)$ can also be extracted from the detection of radial BAO features. Gaztañaga et al. [37] first obtained two $H(z)$ data points using the BAO peak position as a standard ruler in the radial direction. Blake et al. [38] further combined the measurements of BAO peaks and the Alcock–Paczynski distortion to find three other $H(z)$ results. Samushia et al. [39] provided a $H(z)$ point at $z = 0.57$ from the BOSS DR9 CMASS sample. Xu et al. [40] used the BAO signals from the SDSS DR7 luminous red galaxy sample to derive another observational $H(z)$ measurement. The $H(z)$ value determined based upon BAO features in the Lyman-α forest of SDSS-III quasars were presented by Delubac et al. [41] and Font-Ribera et al. [42], which are the farthest precisely observed $H(z)$ results so far. Alam et al. [43] obtained three $H(z)$ measurements with cosmological analysis of the DR12 galaxy sample.

Moreover, Liu et al. [27] present a new method of measuring Hubble parameter by using the anisotropy of luminosity distance, and the analysis of gravitational wave of neutron star binary system.

After evaluating these data points from [44,45], we combine these 43 OHD and present them in Table 1 and mark them in Fig. 1. Note that it is obvious that the cosmic chronometer method is completely model-independent, and one may misjudge the radial BAO method to be dependent of model since they involve in some fiducial ΛCDM models. However, in fact, the fiducial models cannot affect the results as mentioned in the references (e.g., see P. 5 of Alam et al. [43]). Moreover, the three $H(z)$ measurements taken from Blake et al. [38] are correlated with each other, and also, the three measurements of Alam et al. [43] are correlated. This fact will affect the choice of binning range afterwards.

We use a ΛCDM model with no curvature term to compare theoretical values of Hubble parameter with the OHD results, with the Hubble parameter given by

$$H(z) = H_0\sqrt{\Omega_{\rm m}(1+z)^3 + 1 - \Omega_{\rm m}}, \tag{3}$$

where cosmological parameters take values from the Planck temperature power spectrum measurements [9]. The best fit value of H_0 is 67.81 km s^{-1} Mpc^{-1}, and $\Omega_{\rm m}$ is 0.308. The theoretical computation of $H(z)$ based upon this ΛCDM is also shown in Fig. 1.

Being independent observational data, $H(z)$ determinations have been frequently used in cosmological research. One of the leading purposes is using them to constrain DE. Jimenez and Loeb [28] first proposed that $H(z)$ measurements can be used to constrain DE EoS at high redshifts. Simon et al. [30] derived constraints on DE potential using $H(z)$ results and supernova data. Samushia and Ratra [46] began applying these measurements to constraining cosmological parameters in various DE models. In the meanwhile, DE evolution came into its own as an active research field in the last twenty years [47–51]. To sum up, the OHD are proved to be very promising towards understanding the nature of DE.

In the next section, we will bin the OHD in Table 1 by using two binning techniques.

3 Binning OHD

As stated by Farooq et al. [45,52], there are two techniques: the weighted mean and median statistics, which can be used to bin Hubble parameter measurements. In [45], they listed

Table 1 The current available OHD dataset. Where I and II represent the cosmic chronometer and the radial BAO size method, respectively, and $H(z)$ is in units of $\mathrm{km\,s^{-1}\,Mpc^{-1}}$ here

z	$H(z)$	Method	References
0.0708	69.0 ± 19.68	I	Zhang et al. (2014) [33]
0.09	69.0 ± 12.0	I	Jimenez et al. (2003) [29]
0.12	68.6 ± 26.2	I	Zhang et al. (2014) [33]
0.17	83.0 ± 8.0	I	Simon et al. (2005) [30]
0.179	75.0 ± 4.0	I	Moresco et al. (2012) [32]
0.199	75.0 ± 5.0	I	Moresco et al. (2012) [32]
0.2	72.9 ± 29.6	I	Zhang et al. (2014) [33]
0.240	79.69 ± 2.65	II	Gaztañaga et al. (2009) [37]
0.27	77.0 ± 14.0	I	Simon et al. (2005) [30]
0.28	88.8 ± 36.6	I	Zhang et al. (2014) [33]
0.35	84.4 ± 7.0	II	Xu et al. (2013) [40]
0.352	83.0 ± 14.0	I	Moresco et al. (2012) [32]
0.38	81.5 ± 1.9	II	Alam et al. (2016) [43]
0.3802	83.0 ± 13.5	I	Moresco et al. (2016) [35]
0.4	95 ± 17.0	I	Simon et al. (2005) [30]
0.4004	77.0 ± 10.2	I	Moresco et al. (2016) [35]
0.4247	87.1 ± 11.2	I	Moresco et al. (2016) [35]
0.43	86.45 ± 3.68	II	Gaztañaga et al. (2009) [37]
0.44	82.6 ± 7.8	II	Blake et al. (2012) [38]
0.4497	92.8 ± 12.9	I	Moresco et al. (2016) [35]
0.47	89 ± 67	I	Ratsimbazafy et al. (2017) [36]
0.4783	80.9 ± 9.0	I	Moresco et al. (2016) [35]
0.48	97.0 ± 62.0	I	Stern et al. (2010) [31]
0.51	90.4 ± 1.9	II	Alam et al. (2016) [43]
0.57	92.4 ± 4.5	II	Samushia et al. (2013) [39]
0.593	104.0 ± 13.0	I	Moresco et al. (2012) [32]
0.6	87.9 ± 6.1	II	Blake et al. (2012) [38]
0.61	97.3 ± 2.1	II	Alam et al. (2016) [43]
0.68	92.0 ± 8.0	I	Moresco et al. (2012) [32]
0.73	97.3 ± 7.0	II	Blake et al. (2012) [38]
0.781	105.0 ± 12.0	I	Moresco et al. (2012) [32]
0.875	125.0 ± 17.0	I	Moresco et al. (2012) [32]
0.88	90.0 ± 40.0	I	Stern et al. (2010) [31]
0.9	117.0 ± 23.0	I	Simon et al. (2005) [30]
1.037	154.0 ± 20.0	I	Moresco et al. (2012) [32]
1.3	168.0 ± 17.0	I	Simon et al. (2005) [30]
1.363	160.0 ± 33.6	I	Moresco (2015) [34]
1.43	177.0 ± 18.0	I	Simon et al. (2005) [30]
1.53	140.0 ± 14.0	I	Simon et al. (2005) [30]
1.75	202.0 ± 40.0	I	Simon et al. (2005) [30]
1.965	186.5 ± 50.4	I	Moresco (2015) [34]
2.34	222.0 ± 7.0	II	Delubac et al. (2015) [41]
2.36	226.0 ± 8.0	II	FontRibera et al. (2014) [42]

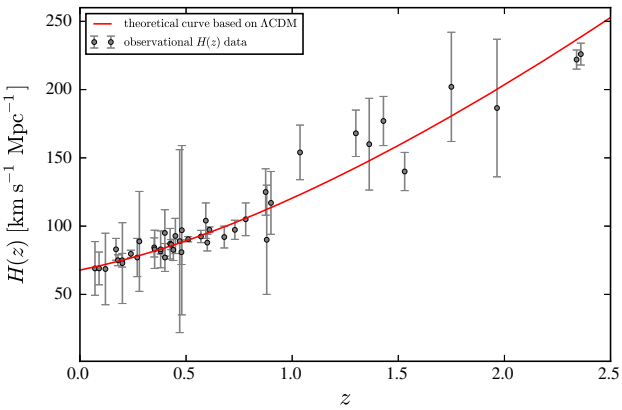

Fig. 1 The full OHD set and theoretical curve of standard flat ΛCDM model. The OHD are represented by gray points along with the uncertainties. The red curve shows theoretical $H(z)$ evolution based upon the adopted ΛCDM model which is described in Sect. 2

two reasons to compute "average" $H(z)$ values for bins in redshift space. On the one hand, the weighted mean technique can indicate whether the original data have error bars inconsistent with Gaussianity. On the other hand, the binned data can more clearly visually illustrate tendencies as a function of redshift, without the assumption of a particular cosmological model.

As for the weighted mean technique, the ideal choice should be a trade-off between bin size and number of measurements per bin that maximizes both quantities. In order to avoid correlations at one bin, we choose 3–4, 4–5, 5–6, and 5–6–7 measurements per bin, which separates the correlated data, and the last four measurements are binned by twos for all the cases.

According to Podariu et al. [53], the weighted mean of $H(z)$ is given by

$$\overline{H}(z) = \frac{\sum_{i=1}^{N}\left(H(z_i)/\sigma_i^2\right)}{\sum_{i=1}^{N} 1/\sigma_i^2}, \tag{4}$$

where $H(z_i)$ and σ_i stand for the Hubble parameter data and the standard deviation for $i = 1, 2, \ldots, N$ measurements in the binning redshift range. Similarly, the corresponding weighted bin redshift $\overline{z}$ and weighted error $\overline{\sigma}$ are as follows,

$$\overline{z} = \frac{\sum_{i=1}^{N}\left(z_i/\sigma_i^2\right)}{\sum_{i=1}^{N} 1/\sigma_i^2}, \tag{5}$$

and

$$\overline{\sigma} = \sqrt{\frac{1}{\sum_{i=1}^{N} 1/\sigma_i^2}}. \tag{6}$$

The goodness of fit for each bin, the reduced χ_ν^2, can be expressed as

$$\chi_\nu^2 = \frac{1}{N-1}\sum_{i=1}^{N}\frac{\left(H(z_i) - \overline{H}(z)\right)^2}{\sigma_i^2}, \tag{7}$$

where the expected value and error of χ_ν are unity and $1/\sqrt{2(N-1)}$. Thus the number of standard deviations which χ_ν deviates from unity for each bin is presented as

$$N_\sigma = |\chi_\nu - 1|\sqrt{2(N-1)}. \tag{8}$$

Non-Gaussian measurements, the presence of unaccounted for systematic errors, or correlations between measurements can result in large N_σ. The weighted mean results for the binned $H(z)$ measurements are listed in Table 2, where the N_σ values are considerably small for all bins, just like results of Farooq et al. [45], hence indicating that the 43 OHD are not inconsistent with Gaussianity.

Since the median statistics technique originally proposed by Gott et al. [54] has a prerequisite which assumes that measurements of a given quantity are independent and that there are no systematic effects, and as previously mentioned the correlative measurements of OHD from Blake et al. [38] and Alam et al. [43] may contaminate the results, we decide to remove these data for the sake of purity. While other measurements are all uncorrelated and independent with each other, they are more sustainable for evaluation and free of negative influence on the binning results. Table 3 displays the results from median statistics technique. After assuming that there is no overall systematic error in the reduced OHD as a whole and all the remaining measurements are independent, it is convenient to use the median statistics to combine the OHD. As the number of the measurements increases and approaches to infinity, the median can be presented as a true value, therefore, this technique has the merits of reducing the effect of outliers of a set of measurements on the estimate of a true median value. Nevertheless, although OHD are a bit of short in quantity as opposed to the large amount of measurements needed to reveal the true value, we still employ this technique for comparison purpose. If N measurements M_i (where $i = 1, 2, \ldots, N$) are considered, the probability of finding the true median between values M_i and M_{i+1} is [54]

$$P_i = \frac{2^{-N}N!}{i!(N-i)!}, \tag{9}$$

where $N!$ represents the factorial of N. After applying this technique to the reduced 37 OHD for binning, we obtain the binned results as listed in Table 3, applying the same binning scheme presented above. The results seem reasonable, but the precision is less than the weighted mean results, which may be caused by the smaller amount of OHD.

Table 2 Weighted Mean Results for 43 Redshift Measurements, where the unit of $H(z)$ is km s^{-1} Mpc^{-1}

Bin	N	z	$H(z)$	$H(z)$ (1σ Range)	$H(z)$ (2σ Range)	N_σ
3 or 4 Measurements per bin						
1	3	0.0895	68.9	59.4–78.5	49.9–88.0	1.98
2	4	0.1847	76.0	73.1–78.9	70.2–81.8	1.12
3	3	0.2412	79.6	77.0–82.2	74.4–84.8	1.56
4	4	0.3776	81.7	79.9–83.5	78.1–85.3	1.85
5	3	0.4095	83.8	76.9–90.7	70.0–97.6	0.61
6	3	0.4329	86.2	83.0–89.4	79.8–92.6	1.02
7	4	0.5086	90.0	88.1–91.9	86.2–93.8	0.98
8	4	0.6024	95.8	94.0–97.6	92.2–99.4	0.06
9	3	0.7201	96.6	91.8–101.4	87.0–106.2	0.71
10	4	0.9287	129.2	118.3–140.1	107.4–151.0	0.07
11	4	1.4301	158.3	149.4–167.2	140.5–176.1	0.05
12	2	1.8331	196.0	164.7–227.3	133.4–258.6	1.07
13	2	2.3487	223.7	218.4–229.0	213.1–234.3	0.88
4 or 5 Measurements per bin						
1	5	0.1664	75.7	72.4–79.0	69.1–82.3	1.18
2	5	0.2321	78.6	76.3–80.9	74.0–83.2	1.55
3	4	0.3776	81.7	79.9–83.5	78.1–85.3	1.85
4	5	0.4276	85.4	82.4–88.4	79.4–91.4	1.26
5	5	0.5074	90.1	88.3–91.9	86.5–93.7	1.33
6	5	0.6061	95.6	93.8–97.4	92.0–99.2	0.23
7	5	0.7681	102.8	97.3–108.3	91.8–113.8	0.45
8	5	1.3647	157.5	149.3–165.7	141.1–173.9	0.32
9	2	1.8331	196.0	164.7–227.3	133.4–258.6	1.07
10	2	2.3487	223.7	218.4–229.0	213.1–234.3	0.88
5 or 6 Measurements per bin						
1	5	0.1664	75.7	72.4–79.0	69.1–82.3	1.18
2	5	0.2321	78.6	76.3–80.9	74.0–83.2	1.55
3	6	0.3785	81.7	80.0–83.5	78.2–85.3	1.75
4	6	0.4276	85.7	82.8–88.6	79.9–91.5	1.89
5	5	0.5263	90.7	89.0–92.4	87.3–94.1	1.13
6	6	0.6312	97.5	95.6–99.4	93.7–101.3	0.51
7	6	1.3128	153.0	145.3–160.7	137.6–168.4	0.28
8	2	1.8331	196.0	164.7–227.3	133.4–258.6	1.07
9	2	2.3487	223.7	218.4–229.0	213.1–234.3	0.88
5, 6 or 7 Measurements per bin						
1	7	0.1767	75.4	72.6–78.2	69.8–81.0	1.80
2	7	0.3333	81.1	79.6–82.6	78.1–84.1	2.27
3	7	0.4288	85.8	82.9–88.7	80.0–91.6	1.71
4	6	0.5247	90.4	88.8–92.0	87.1–93.7	0.89
5	7	0.6331	97.7	95.8–99.6	93.9–101.5	0.55
6	5	1.3647	157.5	149.3–165.7	141.1–173.9	0.32
7	2	1.8331	196.0	164.7–227.3	133.4–258.6	1.07
8	2	2.3487	223.7	218.4–229.0	213.1–234.3	0.88

Table 3 Median statistics results for 37 reduced Redshift measurements, where the unit of $H(z)$ is km s^{-1} Mpc^{-1}

Bin	N	z	$H(z)$	$H(z)$ (1σ Range)	$H(z)$ (2σ Range)
3 or 4 Measurements per bin					
1	3	0.09	69.0	49.3–88.7	29.6–108.4
2	4	0.189	75.0	68.5–81.5	62.0–88.0
3	3	0.27	79.7	65.7–93.7	51.7–107.7
4	3	0.352	83.0	69.5–96.5	56–110.0
5	4	0.4125	86.8	76.1–97.5	65.4–108.2
6	4	0.474	90.9	53.5–128.4	16.0–165.8
7	4	0.6365	98.2	88.2–108.2	78.2–118.2
8	4	0.89	121.0	99.5–142.5	78.0–164.0
9	4	1.3965	164.0	146.5–181.5	129.0–199.0
10	4	2.1525	212.0	188.0–236.0	164.0–260.0
4 or 5 Measurements per bin					
1	5	0.12	69.0	57.0–81.0	45.0–93.0
2	5	0.24	77.0	63.0–91.0	49.0–105.0
3	5	0.3802	83.0	69.5–96.5	56.0–110.0
4	5	0.4497	87.1	75.9–98.3	64.7–109.5
5	5	0.593	97.0	85.0–109.0	73.0–121.0
6	4	0.89	121.0	99.5–142.5	78.0–164.0
7	4	1.3965	164.0	146.5–181.5	129.0–199.0
8	4	2.1525	212.0	188.0–236.0	164.0–260.0
4, 5 or 6 Measurements per bin					
1	5	0.12	69.0	57.0–81.0	45.0–93.0
2	5	0.24	77.0	63.0–91.0	49.0–105.0
3	5	0.3802	83.0	69.5–96.5	56.0–110.0
4	6	0.4598	88.1	76.0–100.2	63.9–112.3
5	6	0.7305	98.2	85.7–110.7	73.2–123.2
6	6	1.3315	157.0	138.0–176.0	119.0–195.0
7	4	2.1525	212.0	188.0–236.0	164.0–260.0
4, 6 or 7 Measurements per bin					
1	7	0.17	72.9	60.9–84.9	48.9–96.9
2	6	0.315	83.0	69.3–96.8	55.5–110.5
3	7	0.43	87.1	75.9–98.3	64.7–109.5
4	7	0.68	97.0	84.0–110.0	71.0–123.0
5	6	1.3315	157.0	138.0–176.0	119.0–195.0
6	4	2.1525	212.0	188.0–236.0	164.0–260.0

Even though the OHD obtained from the BAO method are model-independent, one can still be confused by the employed fiducial models. Therefore, to avoid the confusion and also for comparison purpose, we decide to exclude the OHD from the BAO method and only consider the cosmic chronometer case, which also have the merit of being independent with each other. Tables 4 and 5 present the results from both binning methods. The results are all reasonable as well, and compared to the full binned OHD, the discrepancies are considerably small, which can be seen as evidence of the validity of the OHD derived from the BAO method. Since the different measurements per bin do not significantly affect the results, we can acknowledge the robustness of the binning methods.

4 Testing the ΛCDM model with $Omh^2(z_2; z_1)$ diagnostic

In our analysis, the validity of $Omh^2(z_2; z_1)$ diagnostic can be tested using $H(z)$ results from cosmological independent measurements. On the basis of the above section, we apply binned OHD from both the weighted mean technique and the

Table 4 Weighted mean results for cosmic chronometer measurements, where the unit of $H(z)$ is km s^{-1} Mpc^{-1}

Bin	N	z	$H(z)$	$H(z)$ (1σ Range)	$H(z)$ (2σ Range)	N_σ
3 or 4 Measurements per bin						
1	3	0.0895	68.9	59.4–78.5	49.9–88.0	1.98
2	4	0.1847	76.0	73.1–78.9	70.2–81.8	1.12
3	3	0.3089	80.6	71.0–91.2	61.5–99.7	1.46
4	4	0.4035	83.6	77.5–89.7	71.3–95.9	1.06
5	4	0.4691	85.0	77.7–92.3	70.4–99.6	1.34
6	3	0.6866	97.7	91.7–103.6	85.8–109.5	0.51
7	3	0.8834	118.8	105.9–131.7	93.0–144.6	0.85
8	4	1.2798	166.6	156.6–176.6	146.6–186.6	1.20
9	3	1.58	149.3	136.5–162.1	123.7–174.9	0.33
3, 4 or 5 Measurements per bin						
1	5	0.1664	75.7	72.4–79.0	69.1–82.3	1.18
2	5	0.2221	76.1	71.7–80.5	67.3–84.9	1.90
3	5	0.412	85.3	79.8–90.8	74.2–96.4	1.17
4	5	0.5897	90.1	84.7–85.5	79.3–100.9	0.70
5	4	0.5074	111.4	102.6–120.2	93.8–129	0.86
8	4	1.2798	166.6	156.6–176.6	146.6–186.6	1.20
9	3	1.58	149.3	136.5–162.1	123.7–174.9	0.33
5 or 6 Measurements per bin						
1	5	0.1664	75.7	72.4–79.0	69.1–82.3	1.18
2	5	0.2221	76.1	71.7–80.5	67.3–84.9	1.90
3	5	0.412	85.3	79.8–90.8	74.2–96.4	1.17
4	5	0.5897	90.1	84.7–85.5	79.3–100.9	0.70
5	5	0.8622	118.3	110.2–126.4	102.2–134.4	0.36
6	6	0.6312	161.1	152.5–169.7	143.9–178.3	0.16

median statistics technique to the two-point $Omh^2(z_2; z_1)$ diagnostic.

If $Om(z_2; z_1)$ is always a constant at any redshifts, then it demonstrates that the DE is of the cosmological constant nature. In order to compare directly with the results from CMB, Sahni et al. [55] introduced a more convenient expression of the two-point diagnostic, i.e.,

$$Omh^2(z_2; z_1) = \frac{h^2(z_2) - h^2(z_1)}{(1+z_2)^3 - (1+z_1)^3}, \tag{10}$$

where $h(z) = H(z)/100$ km s^{-1} Mpc^{-1}. The binned $H(z)$ points calculated based upon the aforementioned binning methods in each case therefore yield $N(N-1)/2$ model-independent measurements of the $Omh^2(z_2; z_1)$ diagnostic, as shown in Figs. 2, 3, 4, 5, 6, 7, where the uncertainty $\sigma_{Omh^2(z_2;z_1)}$ can be expressed as follows,

$$\sigma^2_{Omh^2(z_2;z_1)} = \frac{4\left(h^2(z_2)\sigma^2_{h(z_2)} + h^2(z_1)\sigma^2_{h(z_1)}\right)}{\left((1+z_2)^3 - (1+z_1)^3\right)^2}. \tag{11}$$

For ΛCDM, we have $Omh^2 \equiv \Omega_{\rm m}h^2$. The value of $\Omega_{\rm m}h^2$ is constrained tightly by the Planck observations to be centered around 0.14 for the base of ΛCDM model fit [9]: the Planck temperature power spectrum data alone gives 0.1426 ± 0.0020, the Planck temperature data with lensing reconstruction gives 0.1415 ± 0.0019, and the Planck temperature data with lensing and external data gives 0.1413 ± 0.0011, all at 1σ confidence level (CL). As stated in [9], we conservatively select 0.1415 ± 0.0019 as the Planck value. If the ΛCDM model can hold, we would expect a constant value of Omh^2 at any redshift intervals. Sahni et al. [55] compared their results with the Planck value to check the validity of the ΛCDM model. From our perspective, we should not follow their goals to test the tension between our results and the Planck value. Instead, we should first consider whether the values of Omh^2 are constant or not. Here we only use the Planck value for comparison purpose.

As shown in Fig. 2, the results from the weighted mean cases, within 1σ confidence interval, are mostly continuous with both being constant (on average) and the Planck value, although some exceptions are presented and the best-fit $Omh^2(\Delta z)$ values fluctuate. Also, as shown in Fig. 3, the results from the median statistic cases are all continuous with both being constant and the Planck value within

Table 5 Median statistics results for cosmic chronometer measurements, where the unit of $H(z)$ is km s^{-1} Mpc^{-1}

Bin	N	z	$H(z)$	$H(z)$ (1σ Range)	$H(z)$ (2σ Range)
3 or 4 Measurements per bin					
1	3	0.09	69.0	49.3–88.7	29.6–108.4
2	4	0.189	75.0	68.5–81.5	62.0–88.0
3	3	0.28	83.0	69.0–97.0	55.0–111.0
4	4	0.4002	85.1	72.7–97.4	60.4–109.8
5	4	0.4741	90.9	53.5–128.4	16.0–165.8
6	3	0.68	104.0	92.0–116.0	80.0–128.0
7	3	0.88	117.0	94.0–140.0	71.0–163.0
8	4	1.3315	164.0	145.0–183.0	126.0–202.0
9	3	1.75	186.5	146.5–226.5	106.5–266.5
3, 4 or 5 Measurements per bin					
1	5	0.12	69.0	57.0–81.0	45.0–93.0
2	5	0.27	77.0	63.0–91.0	49.0–105.0
3	5	0.4004	87.1	74.2–100.0	61.3–112.9
4	5	0.48	92.0	79.0–105.0	66.0–118.0
5	4	0.8775	111.0	91.0–131.0	71.0–151.0
6	4	1.3315	164.0	145.0–183.0	126.0–202.0
7	3	1.75	172.5	146.5–226.5	106.5–266.5
5 or 6 Measurements per bin					
1	5	0.12	69.0	57.0–81.0	45.0–93.0
2	5	0.27	77.0	63.0–91.0	49.0–105.0
3	5	0.4004	87.1	74.2–100.0	61.3–112.9
4	5	0.48	92.0	79.0–105.0	66.0–118.0
5	5	0.88	117.0	97.0–137.0	77.0–157.0
6	6	1.48	172.5	146.7–198.3	120.9–224.1

1σ confidence interval. Note that these results are not continuous redshift intervals, it only shows the differences for different Δz. Therefore, it would be useful if we plot the continuous results alone to extrapolate the outcomes. Then we illustrate these results with the binned OHD from both binning methods in Fig. 4, which shows that the values of Omh^2 for both binning methods fluctuate as the continuous redshift intervals change. The difference between the results from the weighted mean binning data and results from mean statistics is that the fluctuations from the former situation are more intense which makes the tendency more distinct from the first four panels of Fig. 4. Thus, it is fair to come up with the conclusion that the validity of ΛCDM is preserved.

Also, after binning the OHD from the cosmic chronometer method, the corresponding Omh^2 results with both binning techniques are demonstrated in Figs. 5, 6, 7. It is evident that the fluctuations of the best-fit Omh^2 values are more intense than the results from full binned OHD for both binning methods. However, on average, the results are constant at 1σ region. Hence, due to the two-point $Omh^2(z_2; z_1)$ diagnostic combined with binned OHD results, the ΛCDM model is favored. However, we note that the error bars of these results are much bigger than the Planck result, therefore we can only conclude that the flat ΛCDM model cannot be ruled out.

5 Conclusions and discussions

In this paper, motivated by the investigations on the nature of DE, we test the validity of ΛCDM with the two-point $Omh^2(z_2; z_1)$ diagnostic by using 43 observational $H(z)$ data (OHD) which are obtained from the cosmic chronometers and BAO methods.

Firstly, instead of direct employment of the OHD on the $Omh^2(z_2; z_1)$ diagnostic, we introduce the two binning methods: the weighted mean and median statistics to reduce the noise in the data. After binning OHD, we conclude that the original OHD are not inconsistent with Gaussianity, and the binned data are all reasonable as Tables 2 and 3 displayed. The OHD derived from the BAO method are not generally considered to be completely model-independent, even though as mentioned above the fiducial models indeed cannot affect the results (e.g., see Alam et al. [43], p. 5), which means the data are model-independent after all. Nevertheless, due to the trust issue raised by some scientists, we also apply the binning method to the OHD derived from the cosmic chronometer method alone as listed in Tables 4 and 5 for comparison. The results all seem reasonable and, compared to the full binned OHD, the discrepancies are considerably small, which can be the indirect evidence for the validity of the OHD derived from the BAO method. Since the different measurements per bin do not significantly affect the results, we can acknowledge the robustness of the binning methods.

Secondly, combined with the set of binned OHD and, we exploit the $Omh^2(z_2; z_1)$ diagnostic to test if the Omh^2 values are constant. From Figs. 2, 3, 4, 5, 6, 7, we find that on average the Omh^2 values are mostly constant at 1 σ confidence interval. Therefore, the flat ΛCDM model is not invalid. However, this does not mean that the dynamical DE models are not worth considering.

It is worth noticing that more independent OHD would bring more accuracy toward the binning methods, which can result in more reliable $Omh^2(z_2; z_1)$ values. Also, as the number of OHD grows, the binned OHD would be more efficient as a data clarification instrument that can be employed on cosmological constraints. OHD with higher precision and larger amounts are needed and valuable.

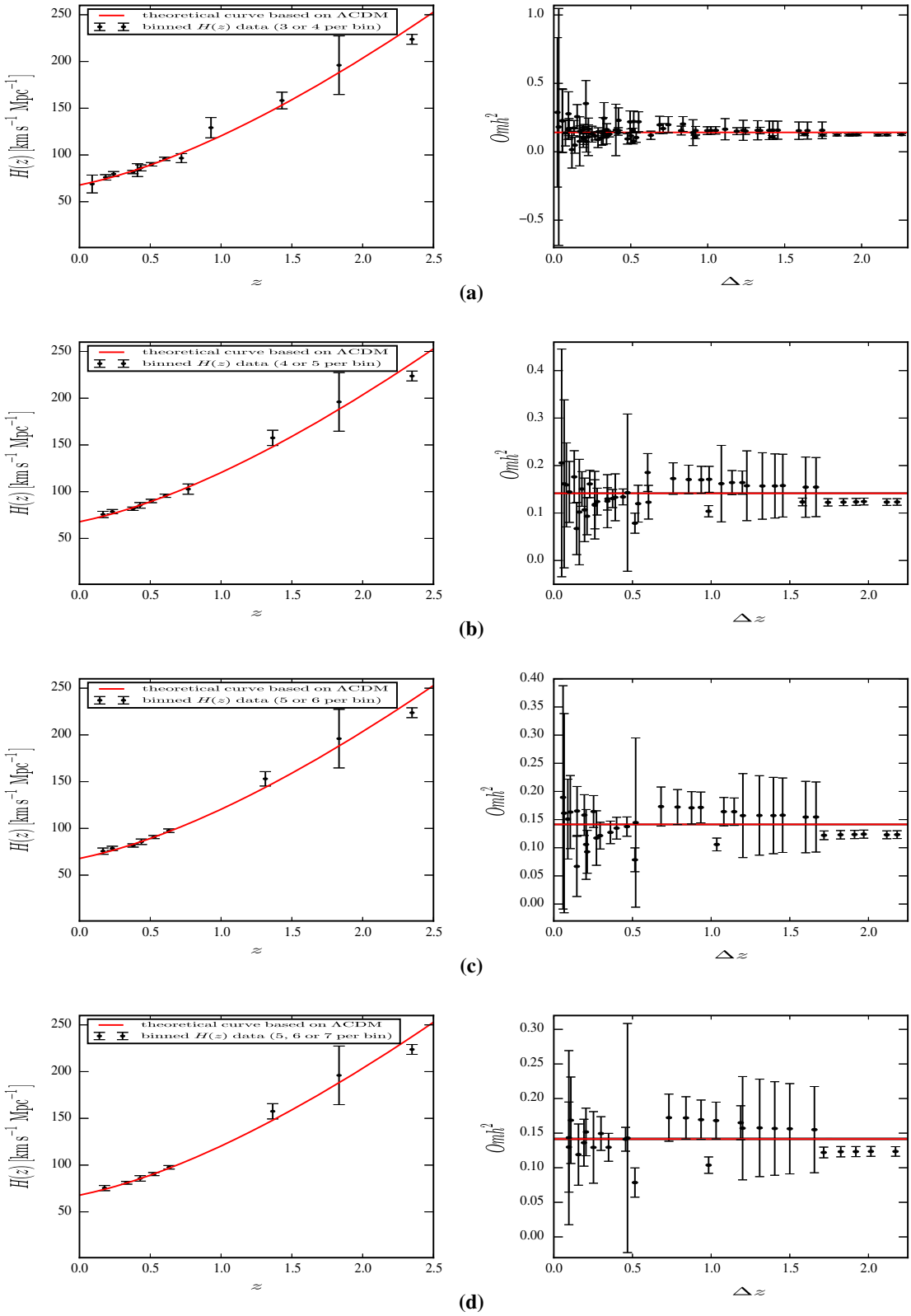

Fig. 2 Binned $H(z)$ data based on full OHD and its corresponding Omh^2 diagnostic values for the weighted mean technique. The panels **a–d** present the 3–4, 4–5, 5–6 and 5–6–7 measurements per bin case, respectively, where the red lines and grey shaded regions in the right panels represent the best-fit value of Omh^2 and its uncertainties retrieved from the Planck CMB data

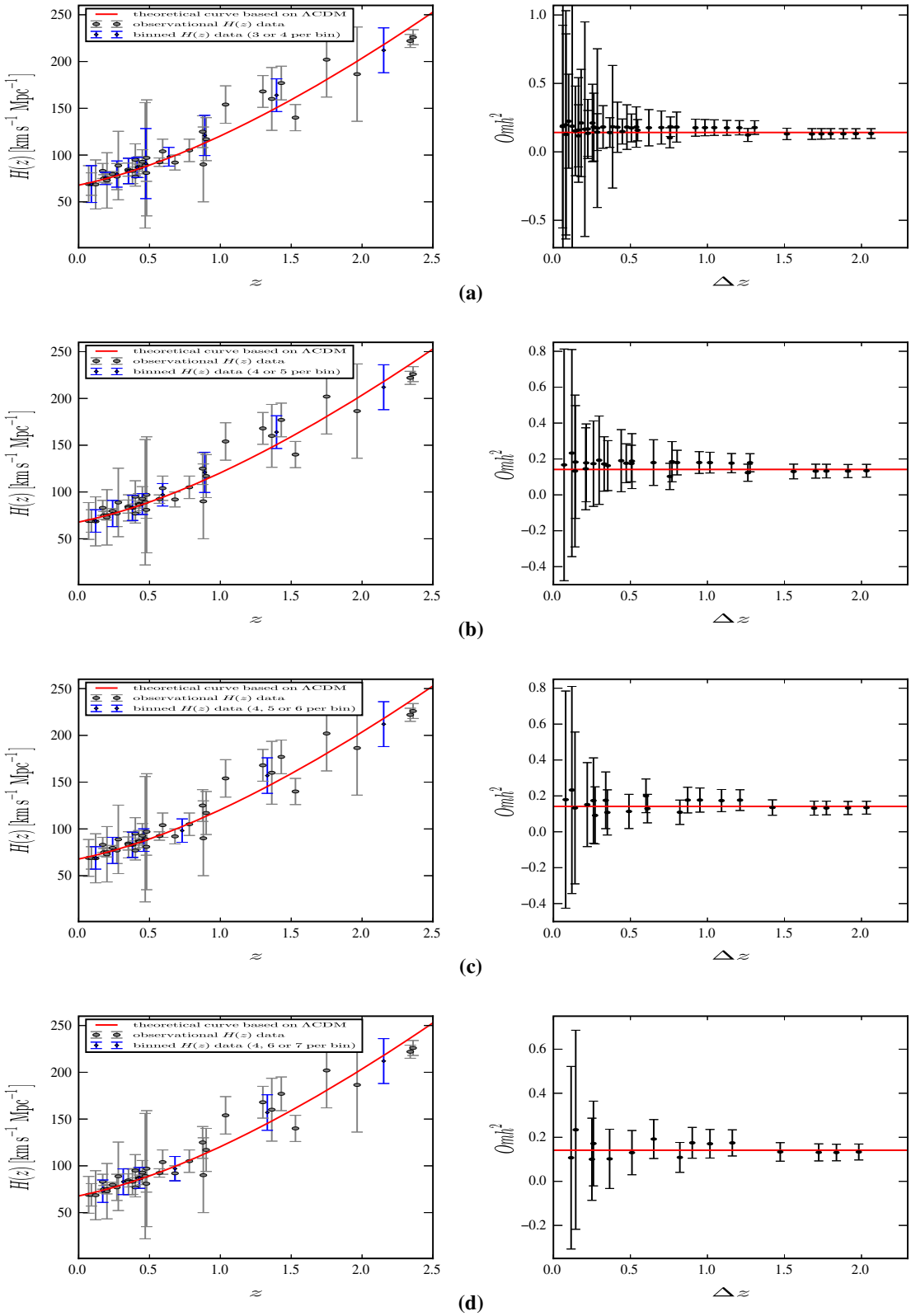

Fig. 3 37 reduced OHD associated with binned data and its corresponding Omh^2 diagnostic values for the median statistics technique. The panels **a**–**d** present the 3–4, 4–5, 4–5–6 and 4–6–7 measurements per bin case, respectively, where the red lines in the right panels represent the best-fit value of Omh^2 retrieved from the Planck CMB data

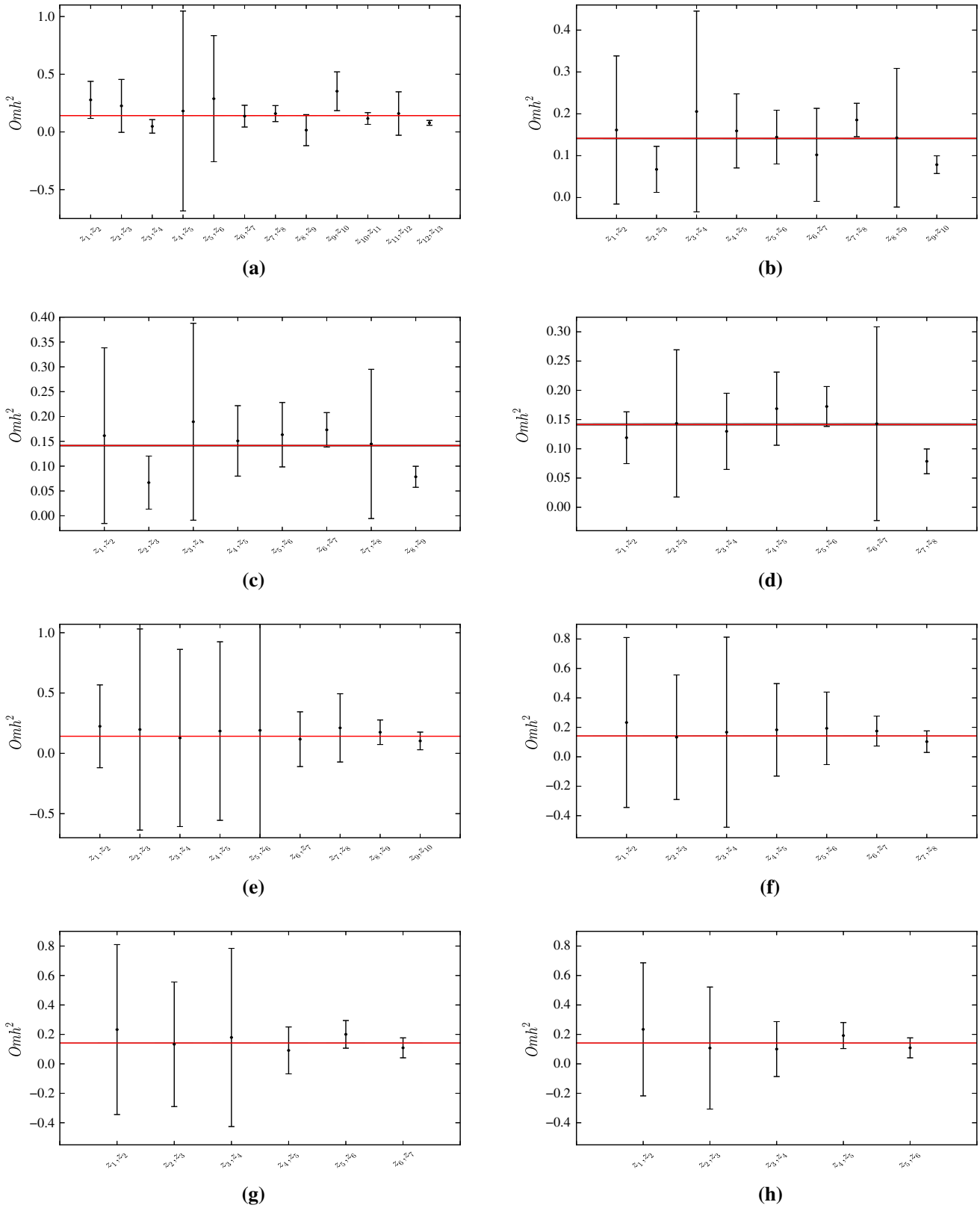

Fig. 4 Omh^2 diagnostic values for both the weighted mean and median statistics techniques with respect to continuous redshifts. The panels **a**–**d** present the weighted mean 3–4, 4–5, 5–6, and 5–6–7 measurements per bin, respectively. The panels **e**–**h** present the median statistics 3–4, 4–5, 4–5–6 and 4–6–7 measurements per bin case, respectively, where the red lines represent the best-fit value of Omh^2 retrieved from the Planck CMB data

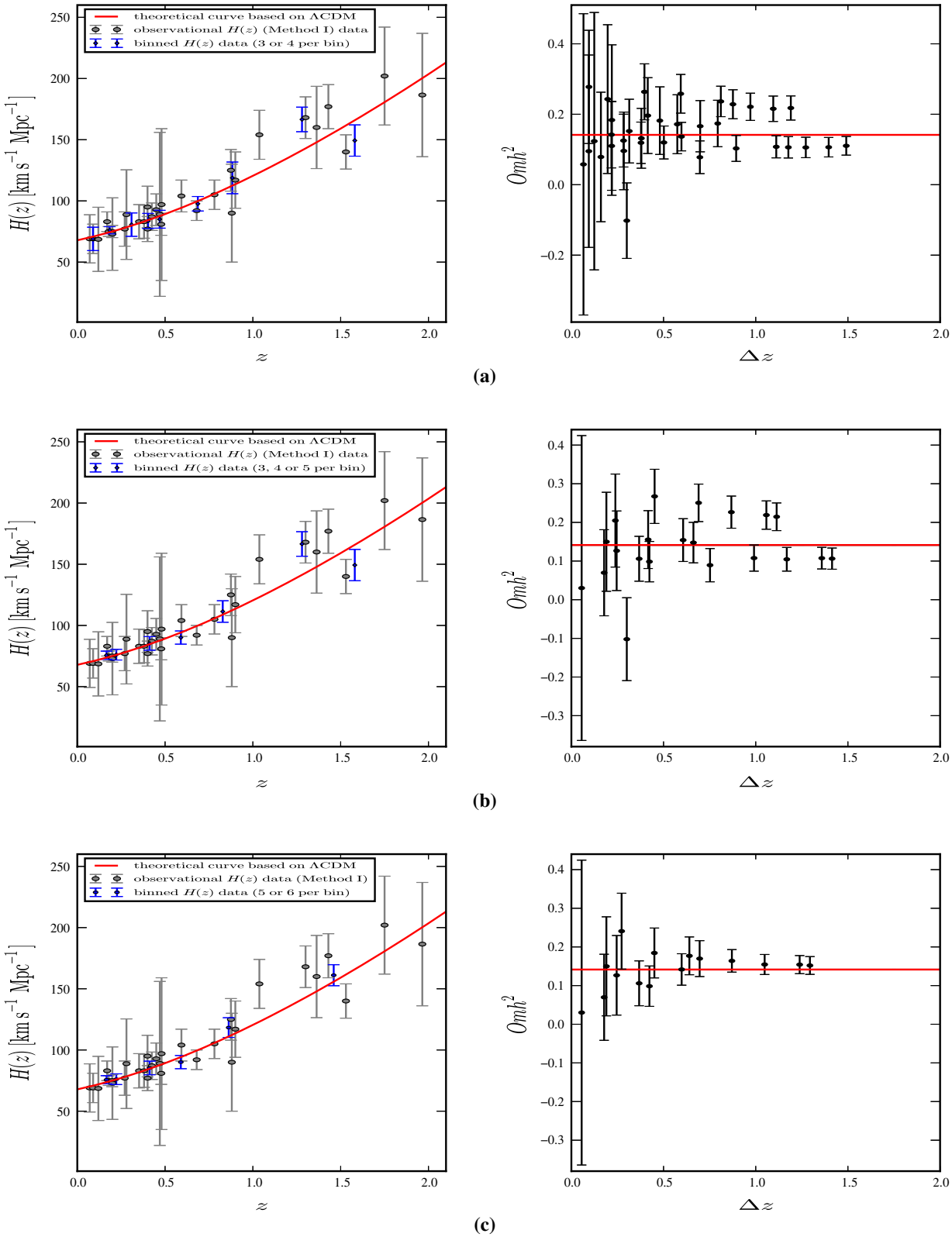

Fig. 5 OHD from the cosmic chronometer method associated with binned data and its corresponding Omh^2 diagnostic values for the weighted mean technique. The panels **a–c** present the 3–4, 3–4–5 and 5–6 measurements per bin case, respectively, where the red lines in the right panels represent the best-fit value of Omh^2 retrieved from the Planck CMB data

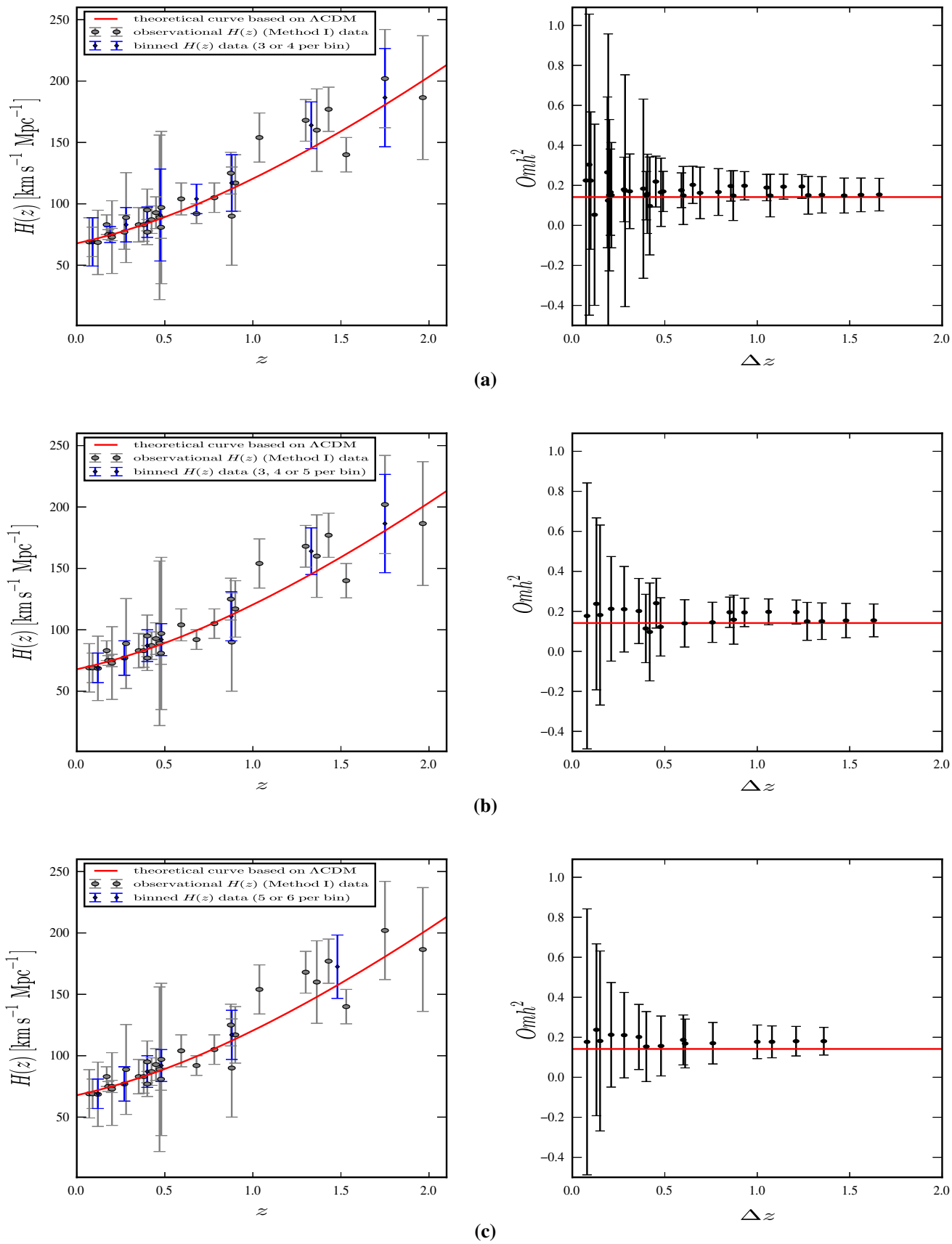

Fig. 6 Same as Fig. 5, but for the median statistics technique

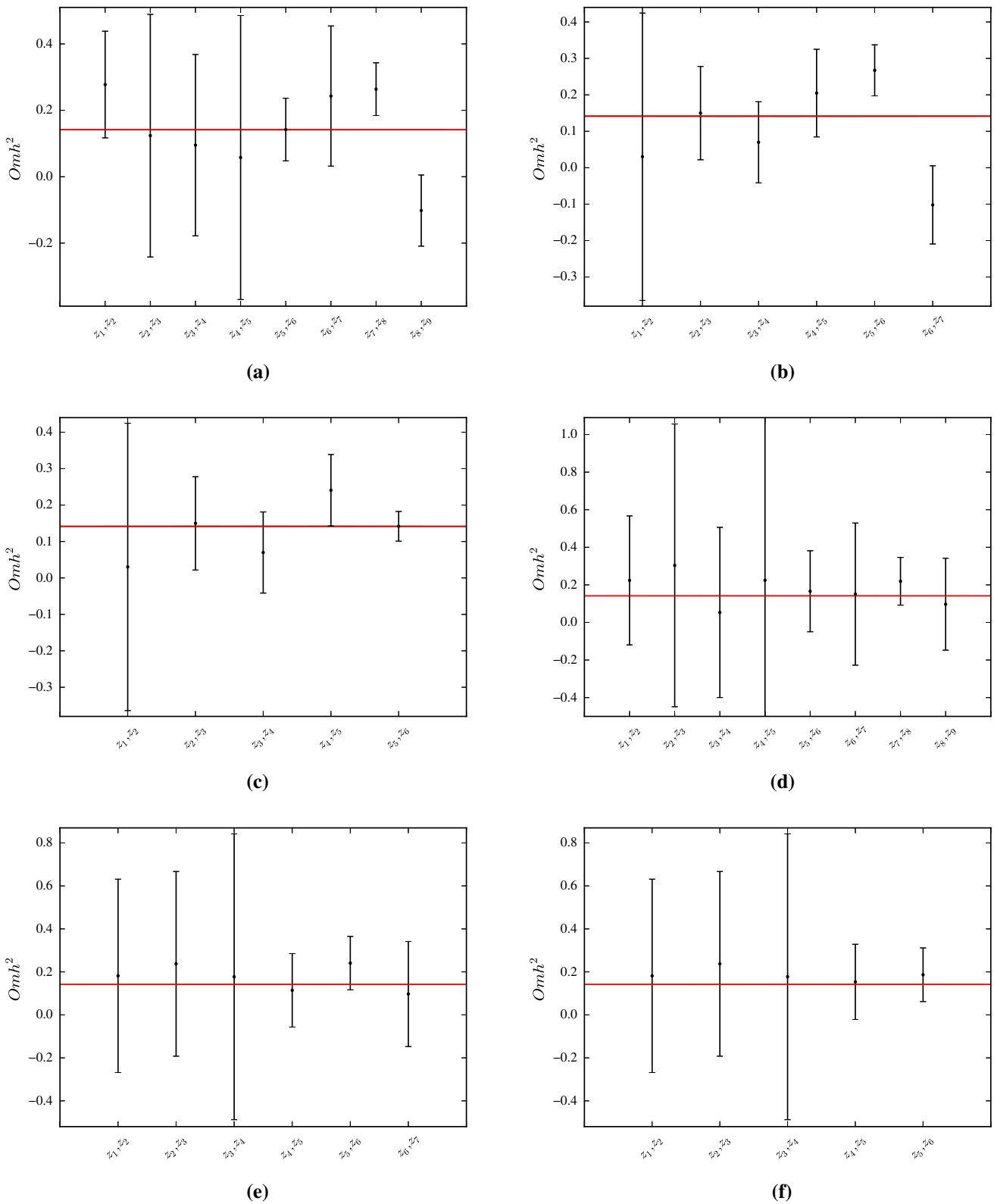

Fig. 7 Same as Fig. 4, but for OHD from the cosmic chronometer method. The panels **a**–**c** present the weighted mean 3–4, 3–4–5, and 5–6 measurements per bin, respectively, and the panels **d**–**f** present the median statistics 3–4, 3–4–5, 5–6 measurements per bin, respectively, where the red lines in the panels represent the best-fit value of Omh^2 retrieved from the Planck CMB data

Acknowledgements We thank the anonymous referee whose suggestions greatly helped us improve this paper. This work was supported by National Key R&D Program of China (2017YFA0402600), the National Natural Science Foundation of China (Grants No. 11573006, 11528306), the Fundamental Research Funds for the Central Universities and the Special Program for Applied Research on Super Computation of the NSFC-Guangdong Joint Fund (the second phase).

Open Access This article is distributed under the terms of the Creative Commons Attribution 4.0 International License (http://creativecommons.org/licenses/by/4.0/), which permits unrestricted use, distribution, and reproduction in any medium, provided you give appropriate credit to the original author(s) and the source, provide a link to the Creative Commons license, and indicate if changes were made.
Funded by SCOAP[3].

References

1. J.A. Frieman, M.S. Turner, D. Huterer, Annu. Rev. Astron. Astrophys. **46**, 385 (2008). https://doi.org/10.1146/annurev.astro.46.060407.145243
2. D.H. Weinberg, M.J. Mortonson, D.J. Eisenstein et al., Phys. Rep. **530**, 87 (2013). https://doi.org/10.1016/j.physrep.2013.05.001
3. A.G. Riess, A.V. Filippenko, P. Challis et al., Astron. J. **116**, 1009 (1998). https://doi.org/10.1086/300499
4. S. Perlmutter, G. Aldering, G. Goldhaber et al., Astrophys. J. **517**, 565 (1999). https://doi.org/10.1086/307221
5. N. Suzuki, D. Rubin, C. Lidman et al., Astrophys. J. **746**, 85 (2012). https://doi.org/10.1088/0004-637X/746/1/85
6. D.J. Eisenstein, I. Zehavi, D.W. Hogg et al., Astrophys. J. **633**, 560 (2005). https://doi.org/10.1086/466512
7. M. Kilbinger, L. Fu, C. Heymans et al., Mon. Not. R. Astron. Soc. **430**, 2200 (2013). https://doi.org/10.1093/mnras/stt041
8. B.A. Benson, T. de Haan, J.P. Dudley et al., Astrophys. J. **763**, 147 (2013). https://doi.org/10.1088/0004-637X/763/2/147
9. Planck Collaboration, P.A.R. Ade, N. Aghanim et al., Astron. Astrophys. **594**, A13 (2016). https://doi.org/10.1051/0004-6361/201525830
10. S. Dodelson, V.K. Narayanan, M. Tegmark et al., Astrophys. J. **572**, 140 (2002). https://doi.org/10.1086/340225
11. W.L. Freedman, B.F. Madore, V. Scowcroft et al., Astrophys. J. **758**, 24 (2012). https://doi.org/10.1088/0004-637X/758/1/24
12. M. Li, X.D. Li, S. Wang et al., Commun. Theor. Phys. **56**, 525 (2011). https://doi.org/10.1088/0253-6102/56/3/24
13. S. Weinberg, Rev. Mod. Phys. **61**, 1 (1989). https://doi.org/10.1103/RevModPhys.61.1
14. I. Zlatev, L. Wang, P.J. Steinhardt, Phys. Rev. Lett. **82**, 896 (1999). https://doi.org/10.1103/PhysRevLett.82.896
15. G.B. Zhao, M. Raveri, L. Pogosian et al., Nat. Astron. **1**, 627 (2017). https://doi.org/10.1038/s41550-017-0216-z
16. B. Ratra, P.J.E. Peebles, Phys. Rev. D **37**, 3406 (1988). https://doi.org/10.1103/PhysRevD.37.3406
17. C. Wetterich, Nucl. Phys. B **302**, 668 (1988). https://doi.org/10.1016/0550-3213(88)90193-9
18. R.R. Caldwell, Phys. Lett. B **545**, 23 (2002). https://doi.org/10.1016/S0370-2693(02)02589-3
19. C. Armendariz-Picon, V. Mukhanov, P.J. Steinhardt, Phys. Rev. Lett. **85**, 4438 (2000). https://doi.org/10.1103/PhysRevLett.85.4438
20. C. Armendariz-Picon, V. Mukhanov, P.J. Steinhardt, Phys. Rev. D **63**(10), 103510 (2001). https://doi.org/10.1103/PhysRevD.63.103510
21. B. Feng, X. Wang, X. Zhang, Phys. Lett. B **607**, 35 (2005). https://doi.org/10.1016/j.physletb.2004.12.071
22. B. Feng, M. Li, Y.S. Piao et al., Phys. Lett. B **634**, 101 (2006). https://doi.org/10.1016/j.physletb.2006.01.066
23. V. Sahni, A. Shafieloo, A.A. Starobinsky, Phys. Rev. D **78**(10), 103502 (2008). https://doi.org/10.1103/PhysRevD.78.103502
24. C. Zunckel, C. Clarkson, Phys. Rev. Lett. **101**(18), 181301 (2008). https://doi.org/10.1103/PhysRevLett.101.181301
25. A. Shafieloo, V. Sahni, A.A. Starobinsky, Phys. Rev. D **86**(10), 103527 (2012). https://doi.org/10.1103/PhysRevD.86.103527
26. T.J. Zhang, C. Ma, T. Lan, Adv. Astron. **2010**, 184284 (2010). https://doi.org/10.1155/2010/184284
27. L. Yang, H.-Y. Wan, T.-J. Zhang, Y.-K. Tang, arXiv:1703.07923
28. R. Jimenez, A. Loeb, Astrophys. J. **573**, 37 (2002). https://doi.org/10.1086/340549
29. R. Jimenez, L. Verde, T. Treu et al., Astrophys. J. **593**, 622 (2003). https://doi.org/10.1086/376595
30. J. Simon, L. Verde, R. Jimenez, Phys. Rev. D **71**(12), 123001 (2005). https://doi.org/10.1103/PhysRevD.71.123001
31. D. Stern, R. Jimenez, L. Verde et al., J. Cosmol. Astropart. Phys. **2**, 008 (2010). https://doi.org/10.1088/1475-7516/2010/02/008
32. M. Moresco, A. Cimatti, R. Jimenez et al., J. Cosmol. Astropart. Phys. **8**, 006 (2012). https://doi.org/10.1088/1475-7516/2012/08/006
33. C. Zhang, H. Zhang, S. Yuan et al., Res. Astron. Astrophys. **14**, 1221 (2014). https://doi.org/10.1088/1674-4527/14/10/002
34. M. Moresco, Mon. Not. R. Astron. Soc. **450**, L16 (2015). https://doi.org/10.1093/mnrasl/slv037
35. M. Moresco, L. Pozzetti, A. Cimatti et al., JCAP **5**, 014 (2016). https://doi.org/10.1088/1475-7516/2016/05/014
36. A.L. Ratsimbazafy, S.I. Loubser, S.M. Crawford et al., Mon. Not. R. Astron. Soc. **467**, 3239 (2017). https://doi.org/10.1093/mnras/stx301
37. E. Gaztañaga, A. Cabré, L. Hui, Mon. Not. R. Astron. Soc. **399**, 1663 (2009). https://doi.org/10.1111/j.1365-2966.2009.15405.x
38. C. Blake, S. Brough, M. Colless et al., Mon. Not. R. Astron. Soc. **425**, 405 (2012). https://doi.org/10.1111/j.1365-2966.2012.21473.x
39. L. Samushia, B.A. Reid, M. White et al., Mon. Not. R. Astron. Soc. **429**, 1514 (2013). https://doi.org/10.1093/mnras/sts443
40. X. Xu, A.J. Cuesta, N. Padmanabhan et al., Mon. Not. R. Astron. Soc. **431**, 2834 (2013). https://doi.org/10.1093/mnras/stt379
41. T. Delubac, J.E. Bautista, N.G. Busca et al., Asrton. Astrophys. **574**, A59 (2015). https://doi.org/10.1051/0004-6361/201423969
42. A. Font-Ribera, D. Kirkby, N. Busca et al., J. Cosmol. Astropart. Phys. **5**, 027 (2014). https://doi.org/10.1088/1475-7516/2014/05/027
43. S. Alam, M. Ata, S. Bailey et al., Mon. Not. R. Astron. Soc. **470**, 2617 (2017). https://doi.org/10.1093/mnras/stx721
44. M. Moresco, F. Marulli, Mon. Not. R. Astron. Soc. **471**, L82 (2017). https://doi.org/10.1093/mnrasl/slx112
45. O. Farooq, F. Ranjeet Madiyar, S. Crandall, B. Ratra, Astrophys. J **835**, 26 (2017). https://doi.org/10.3847/1538-4357/835/1/26
46. L. Samushia, B. Ratra, Astrophys. J. Lett. **650**, L5 (2006). https://doi.org/10.1086/508662
47. V. Sahni, A. Starobinsky, Int. J. Mod. Phys. D **9**, 373 (2000). https://doi.org/10.1142/S0218271800000542
48. S.M. Carroll, Living Rev. Relativ. **4**, 1 (2001). https://doi.org/10.12942/lrr-2001-1
49. P.J. Peebles, B. Ratra, Rev. Mod. Phys. **75**, 559 (2003). https://doi.org/10.1103/RevModPhys.75.559
50. E.J. Copeland, M. Sami, S. Tsujikawa, Int. J. Mod. Phys. D **15**, 1753 (2006). https://doi.org/10.1142/S021827180600942X
51. T. Clifton, P.G. Ferreira, A. Padilla et al., Phys. Rep. **513**, 1 (2012). https://doi.org/10.1016/j.physrep.2012.01.001
52. O. Farooq, S. Crandall, B. Ratra, Phys. Lett. B **726**, 72 (2013). https://doi.org/10.1016/j.physletb.2013.08.078

53. S. Podariu, T. Souradeep, J.R. Gott et al., III, Astrophys. J. **559**, 9 (2001). https://doi.org/10.1086/322409
54. J.R. Gott III, M.S. Vogeley, S. Podariu, B. Ratra, Astrophys. J. **549**, 1 (2001). https://doi.org/10.1086/319055
55. V. Sahni, A. Shafieloo, A.A. Starobinsky, Astrophys. J. Lett. **793**, L40 (2014). https://doi.org/10.1088/2041-8205/793/2/L40